Anisotropic magnetic, magnetocaloric properties, and critical behavior studies of CVT-grown single-crystalline $Fe_{3-x}GeTe_2$

Rosni Roy and Rajib Mondal*

UGC-DAE Consortium for Scientific Research, Kolkata Centre, LB-8, Sector III, Bidhannagar, Kolkata 700 106, India

(Received 7 June 2023; revised 13 December 2023; accepted 19 December 2023; published 12 January 2024)

A comprehensive study of magnetic, room-temperature Mössbauer spectroscopic, room-temperature Raman spectroscopic, magnetocaloric, and critical behavior properties of chemical vapor transport (CVT) grown single-crystalline $Fe_{3-x}GeTe_2$ ($x \approx 0.3$) (F3GT) have been performed. The single crystal of F3GT has been formed in a van der Waals force bonded layered compound. The compound crystallizes in hexagonal crystal structure with space group $P6_3/mmc$. Temperature variation of dc and ac magnetic susceptibility of F3GT reveals a paramagnetic to ferromagnetic transition at ≈180 K (T_C). Field variation of magnetic isotherm in the magnetically ordered state at 5 K reveals strong anisotropy with crystallographic c axis as the easy axis of magnetization. A weak itinerant behavior of Fe spins is also ascertained from the magnetization studies. Magnetocaloric effect in terms of isothermal magnetic entropy change has been estimated to be ≈ −2.6 J/kg-K near T_C for a field change of 100 kOe along crystallographic c direction. The magnetic transition at T_C is found to be of second order. Critical behavior analysis performed for the easy magnetization axis direction in CVT-grown F3GT by modified Arrott plots and Kouvel-Fisher technique suggests that this system does not belong to a particular universality class. However, the critical exponents assume values $\beta = 0.321$, $\gamma = 1.179$, and $\delta = 4.67$. Isothermal magnetization curves at different temperatures in the closed vicinity of ferromagnetic transition of F3GT obey the scaling hypothesis using the estimated critical exponents wherein the magnetization vs field data below and above magnetic transition collapse onto two branches of the universal curves. The critical behavior analyses confirm the weak itinerant ferromagnetic long-range-type interaction due to itinerant 3d electrons and the interaction is very close to the three-dimensional Heisenberg type, wherein the occurrence of long-range-type interaction between the magnetic spins decays as $J(r) \approx r^{-4.74}$ in F3GT.

DOI: 10.1103/PhysRevB.109.024416

I. INTRODUCTION

The discovery of graphene in 2004 opens the flood gate of research interest in the area of quasi-two-dimensional materials which played a significant role in recent times owing to their novel physical properties and other potential applications [1–9]. A lot of research interests have grown in investigating low-dimensional magnetic materials with ferromagnetic nature at room temperature for developing the next-generation spintronic devices. In this context, the magnetic van der Waals materials have opened up a versatile platform owing to some of their appealing properties like strong electron correlations, unusual magnetic domain structures, anomalous Hall effect, Kondo lattice behavior, strong magnetocrystalline anisotropy, etc. [10–13]. Two-dimensional van der Waals bonded layered materials can be mechanically exfoliated down to a few layers even to a monolayer which are the building blocks for heterostructures for applications in spin-based technologies. In van der Waals bonded layered materials, different layers are stacked by weak van der Waals force and layers can be cleaved by mechanical exfoliation. This weak force arises as a result of disparity between interlayer and intralayer bonding forces [14–17]. The Mermin-Wagner theorem states that long-range-type magnetic order in low-dimensional material at a finite temperature is not possible owing to the absence of spontaneous symmetry breaking [18]. However, interestingly two-dimensional van der Waals materials, for example, CrX_3 (where X = Cl, Br, I), $CrXTe_3$ (where X = Si, Ge), etc., which are extensively studied and identified as promising candidates to exhibit long-range magnetism down to monolayers. Despite the fact that these van der Waals materials possess long-range magnetism down to a monolayer, their applications are inhibited due to the low magnetic transition temperature [3,19–23]. There are always quests for searching new magnetic van der Waals materials having high ferromagnetic Curie temperatures. Of late, there is the discovery of a family of magnetic van der Waals materials Fe_nGeTe_2 (where n = 3, 4, 5) which are found to exhibit Curie temperatures ranging from 140 K to more than room temperature which are higher when compared to the other ferromagnetic van der Waals bonded layered materials [24–31]. The iron concentration n in these materials plays a decisive role in their variety and richness of physical properties. Among them, the material Fe_3GeTe_2 has become a point of interest due to some of its intriguing characteristics like magnetocrystalline anisotropy counteracts the fluctuations due to thermal energy and favors two-dimensional (2D) magnetism in Fe_3GeTe_2 [24]. The single crystal of Fe_3GeTe_2 having dimensions of a few millimeters can be grown by either chemical vapor transport (CVT) or high-temperature solution growth technique

*Corresponding author: mondal.rajib1988@gmail.com; rmondal@csr.res.in

[24,30]. The material has a wide range of ferromagnetic Curie temperatures ranging from 140 to 230 K depending upon crystal-growth technique and stoichiometric concentration of iron present in them [24,25]. The CVT-grown crystal is known to exhibit higher ferromagnetic Curie temperature compared to the flux-grown counterpart [24,25,30]. In addition to that, the vacancy in an iron site also reduces the ferromagnetic Curie temperature and influences the physical properties [25]. In this work, a CVT-grown $Fe_{3-x}GeTe_2$ (here onward F3GT), where $x \approx 0.3$ is the vacancy present in the iron site, has been studied for magnetic and other physical property characterizations. The material consists of $Fe_{3-x}Ge$ slabs separated by van der Waals bonded Te layers. There are two inequivalent Fe sites Fe1 and Fe2 forming a noncoplanar hexagonal network in each $Fe_{3-x}Ge$ slab. Unit cells of F3GT form hexagonal lattice structure which belongs to $P6_3/mmc$ space group (No. 194) [24,32]. Mössbauer spectroscopic studies on a F3GT sample reveal the iron vacancy in one of the sites. However, there is no existence of any iron atom in the interlayer space [30,35]. May *et al.* reported the phase stability and magnetic structure of $Fe_{3-x}GeTe_2$ and made a very crucial phase diagram [25]. A significant change in magnetic moment in Fe1 site has been reported upon iron vacancy in $Fe_{3-x}GeTe_2$. A substantial reduction in ferromagnetic Curie temperature and the localized moments with increasing iron vacancy have been reported. The magnetic phase diagram by May *et al.* reported the influence of iron vacancy on the overall magnetism in $Fe_{3-x}GeTe_2$ system [25].

The presently studied CVT-grown F3GT crystal undergoes a ferromagnetic to paramagnetic transition at 179.8 K (T_C) which is in contrast to the F3GT crystal with no iron vacancy ($T_C = 230$ K) [24,25,32]. It is well known that iron vacancy concentration plays a very crucial role in determining the type of interlayer exchange interaction in these iron-based germanium telluride series. In order to figure out the nature of ferromagnetic to paramagnetic transition and type of interaction in terms of range and dimensionality present in the system on the microscopic level, critical behavior analysis study by various methods, like, modified Arrott plot, Kouvel-Fisher method, and critical isotherm analysis, have been performed for F3GT crystals with and without vacancy grown either by CVT or flux method [28–31]. Liu *et al.* reported the critical behavior of CVT-grown F3GT crystal with ferromagnetic transition at 215.1 K and found the critical exponents to be $\beta = 0.327$, $\gamma = 1.079$, and $\delta = 4.30$ [29]. On the other hand, the sample $Fe_{3-x}GeTe_2$ ($x \approx 0.36$) grown by the self-flux method as reported by Liu *et al.* showed ferromagnetic transition at 152 K and the critical exponents are reported to be $\beta = 0.374$, $\gamma = 1.273$, and $\delta = 4.40$ [30]. The critical behavior of Fe_4GeTe_2 with ferromagnetic transition at 270.2 K, as reported by Mondal *et al.*, resulted the critical exponents to be $\beta = 0.33$, $\gamma = 1.17$, and $\delta = 4.54$ [28]. Li *et al.* reported the critical exponents of Fe_5GeTe_2 to be $\beta = 0.351$, $\gamma = 1.413$, and $\delta = 5.03$ with $T_C = 273.7$ K [31]. It is evident from the literature report that the iron concentration and/or iron vacancy in Fe_nGeTe_2 ($n = 3,4,5$) plays a significant role in determining the magnetic exchange interaction and the itinerancy of ferromagnetic behavior which motivated us to perform a comprehensive study of magnetic, magnetocaloric, and critical behavior study of our CVT-grown single-crystalline F3GT having $T_C = 179.8$ K.

II. EXPERIMENTAL DETAILS

The single crystals of F3GT were grown by chemical vapor transport method using iodine as transporting agent. Stoichiometric mixture of high-purity elemental Fe (Alfa Aesar, 99.99%), Ge (Alfa Aesar, 99.999%), Te (Alfa Aesar, 99.999%) in the ratio of 3:1:2 was sealed in a cleaned and evacuated quartz ampoule along with 2 mg/cc iodine (Alfa Aesar, 99.999%) as transporting agent material. The sealed quartz tube was then kept in a horizontal gradient tubular furnace and a temperature gradient was created by maintaining 750 °C at the hot end and 700 °C at the cold end of the quartz tube to grow the single crystal by chemical vapor transport method. After completion of the growth, flat shiny hexagonal-shaped single crystals of dimensions $\sim 2 \times 2 \times 0.35$ mm^3 as shown in the inset of Fig. 1(a) were obtained in the cold end of the quartz tube. Energy dispersive x-ray fluorescence (EDXRF) experiments were done on few crystals to check nominal composition of the crystal. Room-temperature x-ray diffraction of the single crystal and powders were performed using a Bruker make D8 advance x-ray diffractometer to check the single-crystalline nature and phase purity, respectively. Room-temperature Raman spectroscopy data were acquired using a HORIBA make LabRAM HR800 Raman spectrometer for a wavelength of 632 nm. A few shiny crystals were crushed and ground to fine powders and the Mössbauer spectroscopy measurement at room temperature was carried out using a Wissel make spectrometer. The Mössbauer spectra were recorded in the transmission geometry using a radiation source ^{57}Co (in Rh matrix) kept at room temperature. The spectrometer was calibrated by using a Mössbauer spectrum of thin iron foil at room temperature and thus all the estimated isomer shift values are in reference to the iron foil spectrum. Temperature and field variation of ac and dc magnetic susceptibility measurements in the temperature range from 5 to 300 K and in magnetic fields up to ±100 kOe were carried out using a vibrating sample magnetometer attached to a 150 kOe Cryogen Free Measurement System of Cryogenic Limited, U.K. Temperature variations of ac magnetic susceptibility of F3GT sample were measured at 91 Hz frequency in an ac field of magnitude 3 Oe.

III. EXPERIMENTAL RESULTS

A. X-ray diffraction studies

Room-temperature x-ray diffraction (XRD) patterns of the as-grown single crystal and powders are shown in Figs. 1(a) and 1(b), respectively. While collecting the XRD pattern of the crystal, a flat shiny plane of the crystal was exposed to the x rays which resulted the peaks only for the (00z) indicating the single-crystalline nature of the material and it further revealed that the flat plane of the crystal represents the *ab* plane as is evident from the morphology of the grown crystals [inset of Fig. 1(a)]. A few crystals were crushed using mortar and pestle into powders to acquire the powder XRD which revealed the phase purity of the material. All the peaks in the obtained XRD pattern could be indexed to

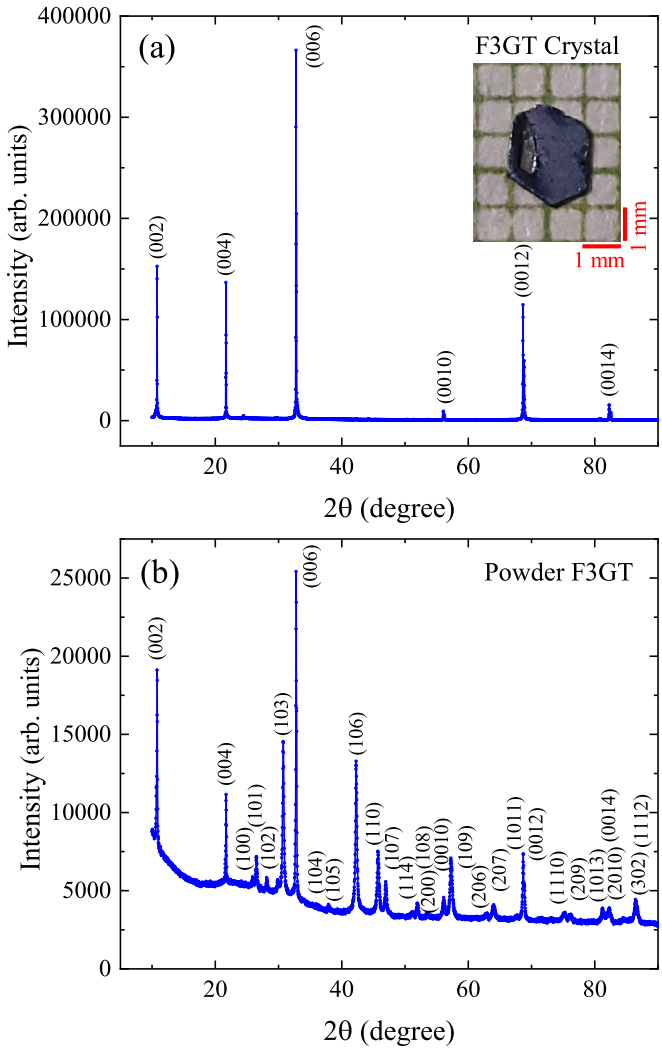

FIG. 1. (a) X-ray diffraction pattern of F3GT single crystal while the flat plane was exposed to the x rays. (The inset shows the image of the grown crystal kept on a graph paper. The smallest box size of the shown graph paper is 1 mm × 1 mm). (b) Room-temperature indexed powder x-ray diffraction pattern of F3GT.

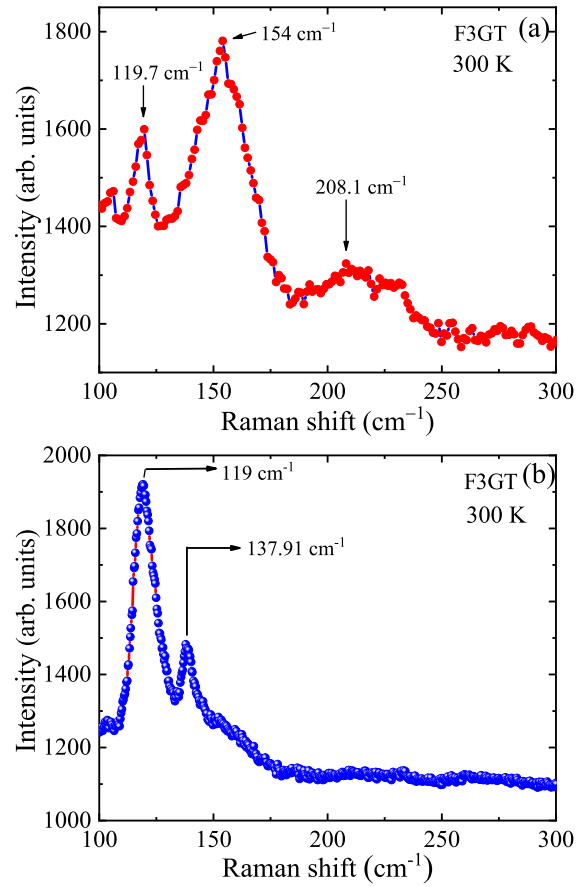

FIG. 2. (a) Room-temperature Raman spectroscopy data of F3GT crystal while the flat *ab* plane was exposed to the laser radiation. Arrows in the plot indicate the Raman active mode of F3GT. (b) Room-temperature Raman scattering spectrum of the F3GT crystal after laser radiation assisted degradation of the crystal surface.

the hexagonal space group and it is evident that the material F3GT crystallizes in hexagonal crystal structure with space group $P6_3/mmc$ (No. 194) which is in conformity with the other reported F3GT crystals grown by different growth techniques and having different iron concentrations [24,25,30,32]. EDXRF experiments performed on the freshly cleaved crystals revealed the composition of the grown crystal to be Fe:Ge:Te of 46.66:19.74:33.60 which resulted the composition of the crystal to be nearly $Fe_{2.7}GeTe_2$.

B. Raman spectroscopy studies

In order to characterize F3GT crystal further, room-temperature Raman spectroscopy data were acquired using a HORIBA make LabRAM HR800 Raman spectrometer. The measurements were performed on a freshly cleaved F3GT crystal and the flat shiny surface of the crystal was exposed to a laser having a wavelength of 632 nm. Since these 2D materials are prone to surface oxidation, the power of the laser was set to keep at a low value in order to avoid any damage to the sample and the scan time for the measurements was fixed to 30 s. The room-temperature Raman spectroscopy data of F3GT crystal are plotted as intensity vs Raman shift as shown in Fig. 2(a). There are three Raman peaks observed at 119.7, 154, and 208.1 cm^{-1} which are in well agreement with previous data for the sample having different iron concentrations and different growth techniques (Raman spectroscopic studies observed at 120, 155, and 240 cm^{-1}) [33,34]. The Raman peak at 154 cm^{-1} is having more intensity than the other peaks which corroborates well with the literature report for the freshly cleaved crystals [33]. Figure 2(b) represents the Raman spectroscopic data of the same F3GT crystal taken after several irradiations which resulted the surface degradation of the crystal. It can be seen from the plot that the Raman peak positions of the degraded crystal are not shifted significantly but the intensity of the peak at ∼120 cm^{-1} is more than of at ∼155 cm^{-1} peak. Also, the third peak is not at all observed in this scenario. This clearly confirms that due to the laser irradiation for longer time, the crystal surface degraded which is also observed and evidenced in the reported literature [33]. This kind of experiment is the fingerprint to check the sample quality. In the literature, it is also reported that 2D van der Waals materials, for example, CrI_3, $CrSiTe_3$,

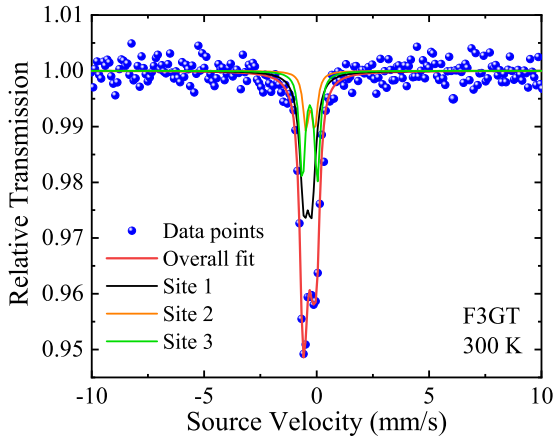

FIG. 3. Room-temperature Mössbauer spectroscopic data of F3GT powder sample with least-square fitting with three different sites.

$CrGeTe_3$, are very much sensitive to ambient conditions and not much stable. Hence, the Raman spectroscopy experiments of F3GT crystal ensure the good crystal quality and it also suggests us to perform any measurements on the freshly cleaved crystals which has been taken into consideration for further experiments.

C. Mössbauer spectroscopy studies

To further characterize the F3GT crystal, the Mössbauer spectroscopic studies at room temperature were performed and the spectrum is shown in Fig. 3. Data were analyzed using a fitting program by using least-square methods. From the structural studies of F3GT, it is well known that F3GT is consisting of $Fe_{3-x}Ge$ slabs separated by van der Waals bonded Te layers and there exist two inequivalent Fe sites, Fe1 and Fe2, forming a noncoplanar hexagonal network in each $Fe_{3-x}Ge$ slab. F3GT crystal is known to be paramagnetic at room temperature and the Mössbauer spectrum of present F3GT powders at 300 K revealed an asymmetric doublet having a broadened part depicting paramagnetic nature. The spectrum at room temperature could be best fitted with three asymmetric paramagnetic doublets instead of two as shown in Fig. 3. The hyperfine splitting parameters provide the information related to the local environment of Fe atoms. In F3GT, the local environment of Fe1 consists of making bond with a Fe1, three Fe2, three Ge and three Te, whereas inequivalent Fe2 makes bonding with nearest three Ge, two Te, and six Fe1. The iron vacancies in F3GT prefer the Fe2 site which leads to distortion in coordination sphere of some Fe1 atoms wherein a different local environment and symmetry are created [35]. This will lead to two equivalent Fe1 sites, denoted by Fe1A and Fe1B, having different local environment. The analysis of the room-temperature spectrum yields the isomer shift values and quadrupole splitting parameters which are tabulated in Table I which are in good agreement with the previous literature reports of F3GT with different iron vacancies grown by different growth techniques [30,35]. The small variations of isomer shift, quadrupole splitting, and the area under the curve in comparison with the previous studies on F3GT system grown either by self-flux method or CVT technique could be attributed to the different iron concentrations [30,35]. The present Mössbauer spectroscopic studies of F3GT at room temperature also ruled out the existence of iron atoms in the interlayer space.

TABLE I. The Mössbauer hyperfine parameters of F3GT obtained from the spectrum measured at room temperature. λ is the experimentally measured isomer shift and Δ is the measured quadrupole splitting of F3GT. The numbers in the parentheses are the error in fitting the spectrum.

Site	Area (mm/s)	Area (%)	λ (mm/s)	Δ (mm/s)
Fe1A	0.028(1)	51.14	0.39(2)	0.35(3)
Fe1B	0.009(1)	16.54	0.28(6)	0.39(9)
Fe2	0.018(1)	32.32	0.30(1)	0.67(2)

D. Magnetization studies

Temperature variation of dc magnetization data of F3GT were measured under zero-field-cooled (ZFC), field-cooled-cooling (FCC), and field-cooled-warming (FCW) conditions in the temperature range of 5–300 K in 1 kOe magnetic field applied along the basal *ab* plane and crystallographic *c* axis as shown in Figs. 4(a) and 4(b). For the magnetization studies under the ZFC protocol, sample was cooled from room temperature to 5 K in the absence of any applied magnetic field and an applied magnetic field of 1 kOe was switched on at 5 K and the dc magnetization data were recorded while warming the sample. In FCC magnetization curve, the dc magnetization data of the sample were acquired while lowering the temperature of the sample from 300 to 5 K in the presence of an applied magnetic field of 1 kOe and again dc magnetization data were recorded from 5 to 300 K without switching off the field in order to obtain the FCW magnetization curve. Magnetization of F3GT crystal along both the crystallographic directions gradually increases from room temperature upon lowering the temperature. Magnetic moment increases rapidly while further lowering the temperature below 200 K and a significant slope change is observed at which a ferromagnetic transition occurred in the material. Below a temperature of about 170 K, magnetization almost shows negligible temperature dependence and the magnetic moment further changes below a temperature of about 50 K. Ferromagnetic transition temperature (T_C) of present F3GT crystal was estimated from temperature dependence first derivative of magnetization with respect to temperature which is found to be at 179.8 K as shown in the inset of Fig. 4(b). The ferromagnetic transition temperature of this CVT-grown F3GT crystal is higher than that of the similar composition crystal grown by the self-flux method [30].

The temperature variations of ac magnetic susceptibility data were acquired for F3GT crystal at 91 Hz frequency in an ac field of magnitude 3 Oe which is shown in the inset of Fig. 4(a). Temperature variations of the real part of ac magnetic susceptibility depict a clear transition at 178.4 K which is close to that obtained from dc magnetic susceptibility data [Fig. 4(a)]. A significant magnetic anisotropy is observed when dc magnetization is measured along the different crystallographic directions. While ZFC magnetiza-

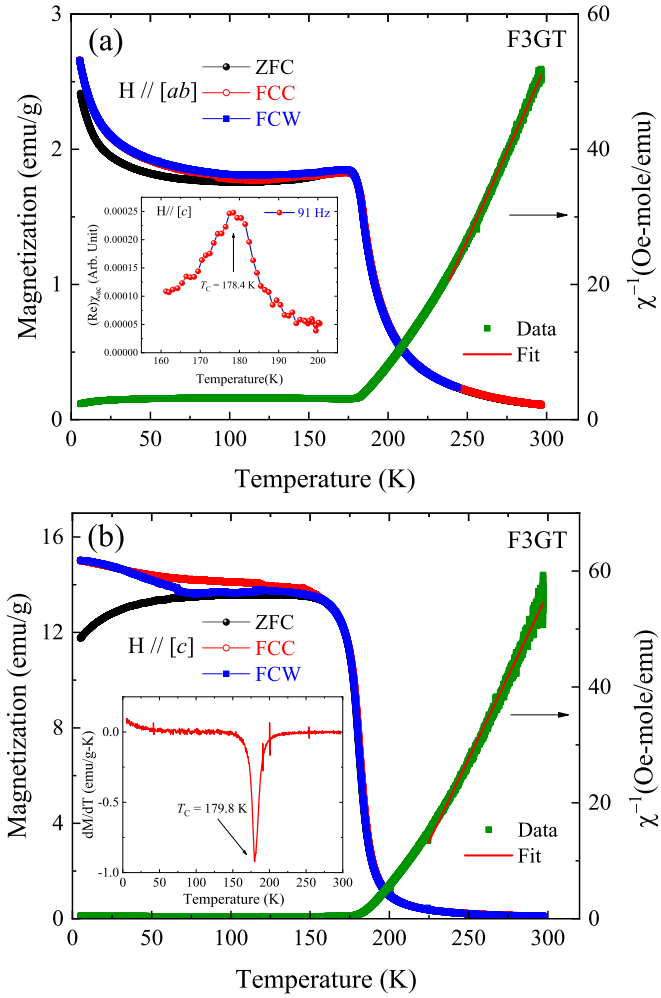

FIG. 4. (a) Temperature variation of magnetization plots of F3GT crystal in 1 kOe magnetic field applied along the *ab* plane under ZFC, FCC, and FCW conditions. The right axis displays the temperature-dependent inverse of magnetic susceptibility data of F3GT crystal for the basal *ab* plane. The inset shows the temperature-dependent ac magnetic susceptibility of F3GT crystal measured for frequency 91 Hz. (b) Temperature variation of magnetization plots of F3GT crystal in 1 kOe magnetic field applied along the *c* direction under ZFC, FCC, and FCW conditions. The right axis displays the temperature-dependent inverse of magnetic susceptibility data of F3GT crystal for the *c* direction. The inset shows the temperature dependence of first derivative of magnetization with respect to temperature of F3GT to obtain the ferromagnetic transition temperature T_C.

tion continues to increase sharply below 10 K when the field is applied along the basal *ab* plane, the ZFC magnetization value decreases below 10 K for the crystallographic *c* direction. Similar behavior was observed in F3GT crystal with different iron vacancies [36]. This behavior could be attributed to the different magnetic spin arrangement or spin coupling along the two crystallographic directions in F3GT crystals. There is significant bifurcation between the ZFC and FC magnetization curves along the *c* direction which is due to the ferromagnetic domain-wall pinning effect. It can also be observed from Figs. 4(a) and 4(b) that there exists a significant thermomagnetic irreversibility leading to thermomagnetic hysteresis between the FCC and FCW magnetization curves in the temperature range from ∼50 to ∼150 K below the ferromagnetic transition when the field is applied along the *c* direction. This kind of behavior is very unusual in the magnetically ordered state of a ferromagnetic material. So there must be an occurrence of a structural and/or an additional magnetic phase transition in this temperature regime. This could be attributed to the antiferromagnetic spin fluctuations that coexist with the ferromagnetism and/or the interplay of local and itinerant 3*d* electrons of magnetic spins of iron in the F3GT system under the study. Recently, there are some remarkable studies in the literature on the F3GT system having different iron vacancy revealing the coexistence of antiferromagnetic spin fluctuations with the ferromagnetism and/or the interplay of local and itinerant electron magnetic spins in the magnetically ordered state [37,38]. The ratio of magnetic moment along the two crystallographic directions in the magnetically ordered state at ∼100 K, M_{ab}/M_c is ∼0.13 indicating large anisotropy and also confirms that the crystallographic *c* direction is the easy magnetization direction which is in conformity with the previously reported F3GT materials with different iron concentrations grown by different growth techniques [24,25,29,30,36]. The inverse of paramagnetic susceptibility data in the temperature range from ∼230 to 298 K of F3GT crystal for 1 kOe field applied along two crystallographic directions could be linearly fitted according to the Curie-Weiss law, as shown in Figs. 4(a) and 4(b). From the linear fit, the calculated values of effective paramagnetic moment (μ_{eff}) and paramagnetic Curie temperature (θ_p) are ≈3.92 μ_B/Fe and +198.9 K, respectively, for applied field parallel to the *ab* plane and the obtained values of the same parameters for applied field parallel to the *c* direction are ≈3.74 μ_B/Fe and +201.7 K, respectively. This obtained value of μ_{eff} of F3GT crystal is in conformity with the values reported in the literature for F3GT materials [25]. The large positive θ_p values along both the crystallographic directions of F3GT indicate the dominant ferromagnetic interaction which is occurring in the present F3GT crystal.

To shed further light on the anisotropic magnetic behavior of the grown F3GT crystal, field variations of isothermal magnetization data at temperatures of 5, 100, 200, and 300 K have been acquired and plotted in Figs. 5(a) and 5(b). In the magnetically ordered state at 5 K, the magnetization saturates for both the basal *ab* plane and the *c* direction with a negligible hysteresis loss, indicating a soft ferromagnetic behavior of F3GT crystal. The saturation magnetizations of F3GT crystal at 5 K along the *ab* plane and the *c* direction are ≈1.25 μ_B/Fe (M_s^{ab}) and ≈1.27 μ_B/Fe (M_s^c), respectively, in 100 kOe fields, which are almost one-half of the saturation magnetic moment of free iron. The values obtained are in good agreement with the reported values of F3GT without any iron vacancy [24]. However, the reduction in saturation magnetization when compared to that of free iron may hint for the itinerant character of iron 3*d* electrons in this compound. Magnetization along the *c* direction (M_c) saturates easier at a low field than along the *ab* plane, indicating the crystallographic *c* direction is the easy axis of magnetization. The magnetic field in which the magnetization almost saturates is denoted as saturation fields which are found to be ∼30 kOe (H_s^{ab}) and ∼3 kOe (H_s^c), respectively, for the *ab* plane and *c*

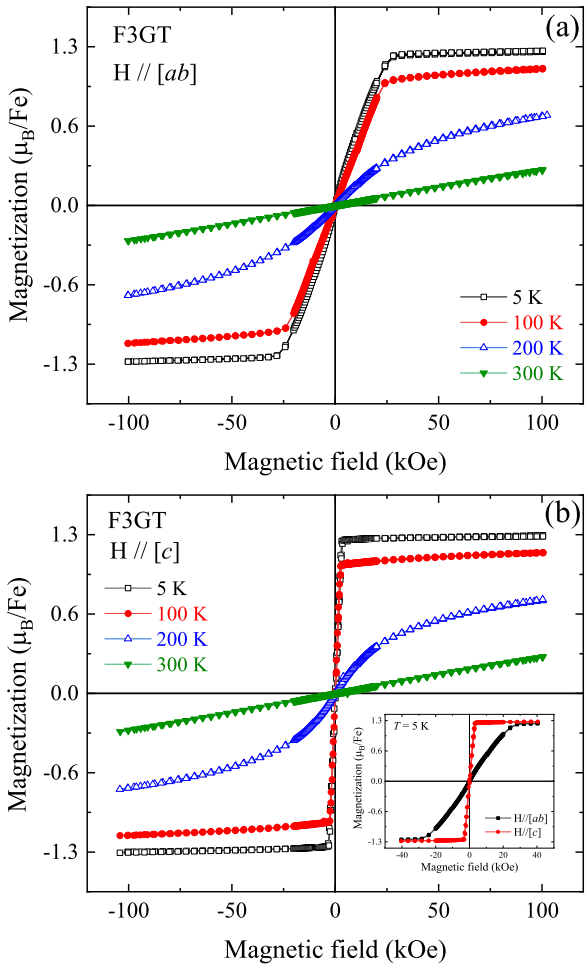

FIG. 5. (a), (b) Magnetic field dependence of isothermal magnetization curves of F3GT crystal taken at temperatures 5, 100, 200, and 300 K, for field applied along *ab* plane and crystallographic *c* direction, respectively. The inset in (b) shows the magnetization vs magnetic field of F3GT crystal at 5 K for the fields up to ±40 kOe applied along the principal crystallographic directions.

direction. The coercive fields of F3GT crystal are found to be ∼88 Oe (H_C^{ab}) and ∼160 Oe (H_C^c), respectively, for the *ab* plane and *c* direction. The obtained saturation magnetization of F3GT crystal is slightly less as compared to the expected value for iron. This kind of discrepancy could be due to the itinerant nature of iron 3*d* electrons in the F3GT crystal. Thus, to check and confirm the degree of itinerant nature of iron 3*d* electrons in this material, the itinerant magnetization model proposed by Rhodes and Wohlfarth has been applied [39,40]. As per this model, one can determine the existence of itinerancy by examining the Rhodes-Wohlfarth ratio (RWR). The RWR of a material can be obtained from the ratio of the magnetization parameters as given by M_c/M_s, where M_s represents the spontaneous magnetization of the material and M_c can be determined from the effective magnetic moment, μ_{eff} from the relation $M_c(M_c + 2) = \mu_{\text{eff}}^2$. For localized moments, the RWR has a value of unity, while for the itinerant electron scenario, the value is greater than unity [39,40]. The calculated values of the RWR of F3GT crystal are found to be ≈2.56 and 2.35 for $H \parallel [ab]$ and $H \parallel [c]$, respectively. These values are slightly smaller in comparison to the RWR value of F3GT without any iron vacancy [24]. However, the obtained RWR values of the present F3GT crystal indicates a weak itinerant electron nature and/or significant spin fluctuation in the magnetic ground state of the system leading to the strong suppression of saturation magnetic moment.

E. Magnetocaloric properties and critical behavior study

Magnetic field-dependent isothermal magnetization data $M(H)$ of F3GT crystal for $H \parallel [ab]$ and $H \parallel [c]$ at a few temperatures in the vicinity of T_C have been collected and plotted in Figs. 6(a) and 6(c), respectively, to explore the magnetocaloric properties of the material. Magnetocaloric effect (MCE) is an intrinsic functional property of a magnetic material in which the heating or cooling is caused by the application or removal of magnetic field, respectively, under adiabatic conditions [41]. Under isothermal conditions, the magnetocaloric effect of a material leads to the change of magnetic entropy of the materials due to the influence of magnetic field [41].

The magnetocaloric effect of a material is analyzed by the estimation of isothermal magnetic entropy change (ΔS_m) and adiabatic temperature change (ΔT_{ad}) of the material which can be deduced from the measurements of field-dependent isothermal magnetization and specific heat in zero and applied magnetic fields of a material. In this study, temperature and magnetic field dependence of ΔS_m data have been calculated from the magnetic field variation isothermal magnetization curves shown in Figs. 6(a) and 6(c) in the vicinity of ferromagnetic transition of F3GT. The calculation of ΔS_m can be performed from the magnetization isotherm data by using the Maxwell's relation used for magnetic materials as given below [41–43]:

$$\left(\frac{\partial S(T,H)}{\partial H}\right)_T = \left(\frac{\partial M(T,H)}{\partial T}\right)_H. \quad (1)$$

Under isothermal conditions, the change in magnetic entropy can be deduced by using the relationships as follows:

$$\Delta S_m(T, \Delta H) = \int_{H_i}^{H_f} \left(\frac{\partial M(T,H)}{\partial T}\right)_H dH \simeq \sum_j \frac{M_{j+1}(T_{j+1},H) - M_j(T_j,H)}{T_{j+1} - T_j} \Delta H, \quad (2)$$

where the initial and final fields are denoted by H_i and H_f, respectively, and M_j and M_{j+1} are the measured value of magnetization in a field H at temperatures T_j and T_{j+1}, respectively [41–43]. The temperature variation of calculated values of ΔS_m of F3GT crystal for $H \parallel [ab]$ and $H \parallel [c]$ for magnetic field changes ΔH up to 100 kOe are displayed in Figs. 6(b) and 6(d), respectively. As can be seen from these figures, the maximum value of isothermal magnetic entropy change $\Delta S_m^{\max}$ is centered near T_C of F3GT as expected for magnetic materials owing to the fact that a maximum entropy change occurs at the order to disorder transition. The obtained values of $\Delta S_m^{\max}$ of F3GT crystal are ≈ −1.4 J/kg K and ≈ −1.7 J/kg K for $\Delta H = 50$ kOe for $H \parallel [ab]$ and $H \parallel [c]$, respectively. $\Delta S_m^{\max}$ of F3GT crystal are ≈ −2.4 J/kg K and ≈ −2.6 J/kg K for $\Delta H = 100$ kOe for $H \parallel [ab]$ and $H \parallel [c]$, respectively. These obtained values are comparable to those of

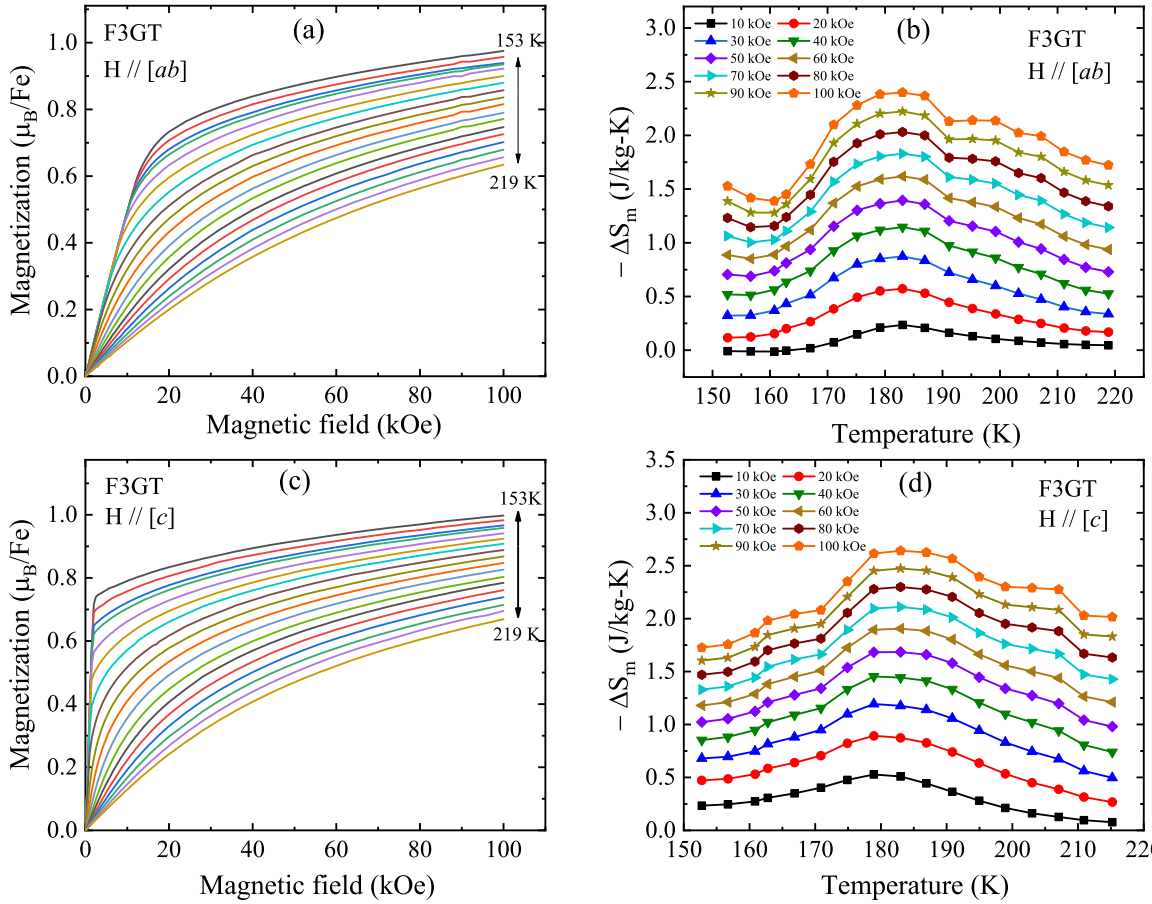

FIG. 6. (a), (c) Magnetization vs magnetic field taken at different temperatures in the close vicinity of ferromagnetic transition of F3GT crystal for field applied along the principal crystallographic directions, *ab* plane and *c* direction, respectively. (b), (d) Plot of the estimation of temperature variation magnetocaloric effect of F3GT crystal in terms of isothermal magnetic entropy change in different field changes for the *ab* plane and *c* direction, respectively.

F3GT crystal with no iron vacancy and other reported F3GT crystals with different iron vacancies [35,44]. The sample under this study displays little more ΔS_m^{max} as compared to the reported F3GT crystal (-1.2 J/kg K for $\Delta H = 50$ kOe) [35,44]. This could be attributed to the presence of slightly different iron concentration in the present material under the study. However, the obtained ΔS_m^{max} value of F3GT is smaller when compared to the same with other two-dimensional ferromagnetic van der Waals bonded layered materials, such as $CrSiTe_3$ (-5.1 J/kg K for $\Delta H = 50$ kOe) [45], $CrGeTe_3$ (-2.6 J/kg K for $\Delta H = 50$ kOe) [45], CrI_3 (-1.6 J/kg K for $\Delta H = 50$ kOe) [46], $CrBr_3$ (-7.2 J/kg K for $\Delta H = 50$ kOe) [47], Cr_5Te_8 (-1.6 J/kg K for $\Delta H = 50$ kOe) [43], Cr_4Te_5 (-2.6 J/kg K for $\Delta H = 50$ kOe) [48]. The nature of the temperature variation of isothermal magnetic entropy change of F3GT in different field changes displays almost symmetric behavior with respect to the magnetic transition thereby indicating the magnetic transition from ferromagnetic to paramagnetic in F3GT is indeed a second-order transition, as shown in Figs. 6(b) and 6(d).

From the previous studies of F3GT single crystals having different iron vacancy grown by different crystal-growth techniques ruled out the occurrence of mean field type magnetic correlation in them which then motivated us to the study of critical behavior and determination of the critical exponents of our F3GT single crystal grown by chemical vapor transport growth technique [29,30]. The determination of critical exponents of a magnetic material undergoing second-order magnetic transition from ferromagnetic to paramagnetic state provides very useful information related to the magnetic phase transition including the range and dimensionality of magnetic exchange interaction associated with the material. The critical behavior of a magnetic material exhibiting a second-order magnetic phase transition can be very well characterized by a set of interrelated parameters called critical exponents from the data of isothermal magnetization curves in the vicinity of magnetic transition [49–53]. In the closed vicinity of ferromagnetic to paramagnetic transition, spin-spin correlation length denoted by ξ diverges which leads to the universal behavior of scaling laws of the spontaneous magnetization (M_S) and the inverse of initial magnetic susceptibility (χ_0^{-1}). For a magnetic material undergoing a second-order magnetic transition from ferromagnetic to paramagnetic state near T_C, the temperature dependence of spontaneous magnetization (M_S) below T_C and the inverse of initial magnetic susceptibility (χ_0^{-1}) above T_C can be very well characterized by a set of static interrelated parameters β, γ, and δ, known as critical exponents which are related to the spontaneous magnetization M_S (magnetization at $H = 0$), initial magnetic susceptibility χ_0 ($\frac{\partial M}{\partial H}$ at $H = 0$) and the isothermal magnetization $M(H)$ at

T_C, respectively, by power laws via the following equations as given below [49–53]:

$$M_S(T) = M_0(-\epsilon)^{\beta}, \quad \epsilon < 0 \tag{3}$$

$$\chi_0^{-1}(T) = \left(\frac{h_0}{M_0}\right)\epsilon^{\gamma}, \quad \epsilon > 0 \tag{4}$$

$$M = DH^{1/\delta}, \quad \epsilon = 0 \tag{5}$$

where $\epsilon = (\frac{T-T_C}{T_C})$ is denoted as the reduced temperature and M_0, (h_0/M_0), and D are the various critical amplitudes associated to the material. According to the hypothesis of scaling theory for a continuous magnetic phase transition, the set of experimental isothermal magnetization $M(H)$ curves measured at different temperatures in the closed vicinity of T_C are expected to collapse onto universal curve and the magnetic equation of state of the system which is function of field H and temperature T can be expressed as the following equation:

$$M(H, \epsilon) = \epsilon^{\beta} f_{\pm}\left(\frac{H}{\epsilon^{\beta+\gamma}}\right). \tag{6}$$

In the above equation, $f_{\pm}$ is a regular function, in which the "+" sign indicates the magnetization data for $T > T_C$ and the "−" sign indicates the magnetization data for $T < T_C$. It has been evidenced in the literature that such a scheme does exist wherein all the experimental isothermal magnetization curves in close vicinity of T_C of the material scales onto two branches of universal curves below and above T_C. This model applied successfully for numerous materials exhibiting ferromagnetic to paramagnetic transition including several two-dimensional magnetic van der Waals materials, for example, $CrSiTe_3$, $CrGeTe_3$, Fe_3GeTe_2, Fe_4GeTe_2, Fe_5GeTe_2, etc. [28–31,54–57]. The dc and ac magnetic susceptibility studies of the present F3GT crystal reveal the occurrence of ferromagnetic to paramagnetic transition at $T_C = 179.8$ and 178.4 K, respectively. In order to characterize the present F3GT crystal for critical behavior study, a set of isothermal magnetization curves in the vicinity of T_C of F3GT at various temperatures from 165 to 197 K for $H \parallel [c]$ were measured and analyzed, as shown in Fig. 7(a). The magnetic field values of the isothermal magnetization curves employed for critical behavior analysis have been corrected for the demagnetization factor using the formula $H = H_{app} - NM$, where N is the demagnetization factor [28,30,58]. The demagnetization factor N has been calculated by using $N = H/M$ from the isothermal magnetization curve of F3GT near low fields at low temperatures (below T_C). For the magnetization isotherm at 165 K, the demagnetization factor N of F3GT is found to be 75. Figure 7(b) displays the conventional M^2 vs H/M plot which is popularly known as the Arrott plot of present F3GT crystal. The evidence of positive slope in M^2 vs H/M data at different temperatures near T_C indicates the occurrence of second-order magnetic transition at T_C of F3GT crystal [Fig. 7(b)]. In the Arrott plot, the positive slope from the M^2 vs H/M data or a positive value of Landau coefficient denoted by $b(T)$ indicates the occurrence of a second-order magnetic transition. The magnetic equation of state for the same in terms of Landau coefficients is expressed as the following equation [59,60]:

$$a(T)M + b(T)M^3 = \mu_0 H. \tag{7}$$

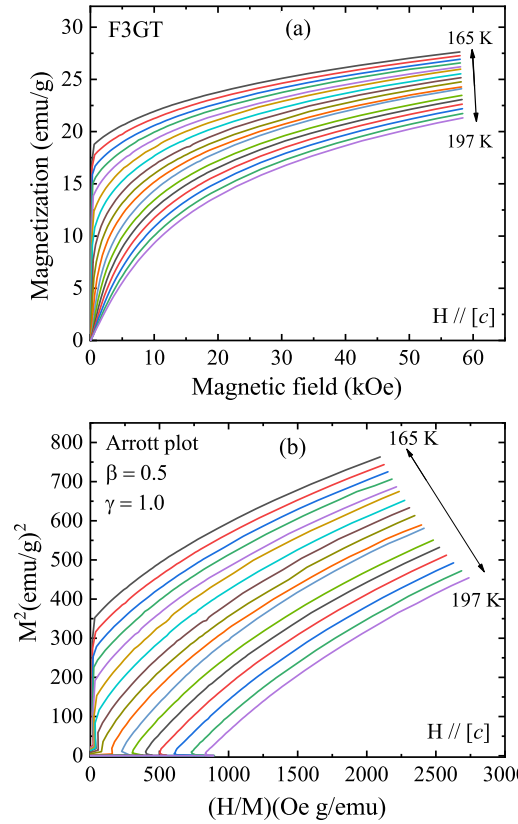

FIG. 7. (a) Magnetic field dependence of isothermal magnetization plot taken at different temperatures in the vicinity of ferromagnetic transition of F3GT for critical behavior studies. The magnetic field axis has been corrected for the demagnetization factor (see details in text). (b) Arrott plot, i.e., M^2 vs H/M plot of F3GT crystal.

As per the above equation of state for a magnetic material, M^2 vs H/M should display a set of parallel straight lines and the curve at T_C passes through the origin. The Arrott plot reveals nonlinear curves which are not parallel to each other in case of a material which does not obey the mean field theory. For those materials, to obtain a set of linear and parallel curves in Arrott plots along with the condition that the curve at T_C in the Arrott plots should pass through the origin, Arrott and Noakes modified the equation of state and proposed a general expression of equation of state related to the critical exponents of a material as given below [61]:

$$\left(\frac{H}{M}\right)^{\frac{1}{\gamma}} = \left(\frac{T - T_C}{T_C}\right) + \left(\frac{M}{M_1}\right)^{\frac{1}{\beta}}. \tag{8}$$

As one can see that following the modified equation of state proposed by Arrott and Noakes, the conventional Arrott plot, i.e., M^2 vs H/M plot, is a case where the critical exponents $\beta = 0.5$ and $\gamma = 1$ are taken into consideration for a material obeying mean field theory [59,60]. The Arrott plot of present F3GT crystal for $H \parallel [c]$ reveals a set of nonlinear curves and the curve near T_C does not pass through the origin [Fig. 7(b)], indicating that the present F3GT does not obey the mean field theory and the critical exponents are different from $\beta = 0.5$ and $\gamma = 1$. To find out the critical exponents for the present

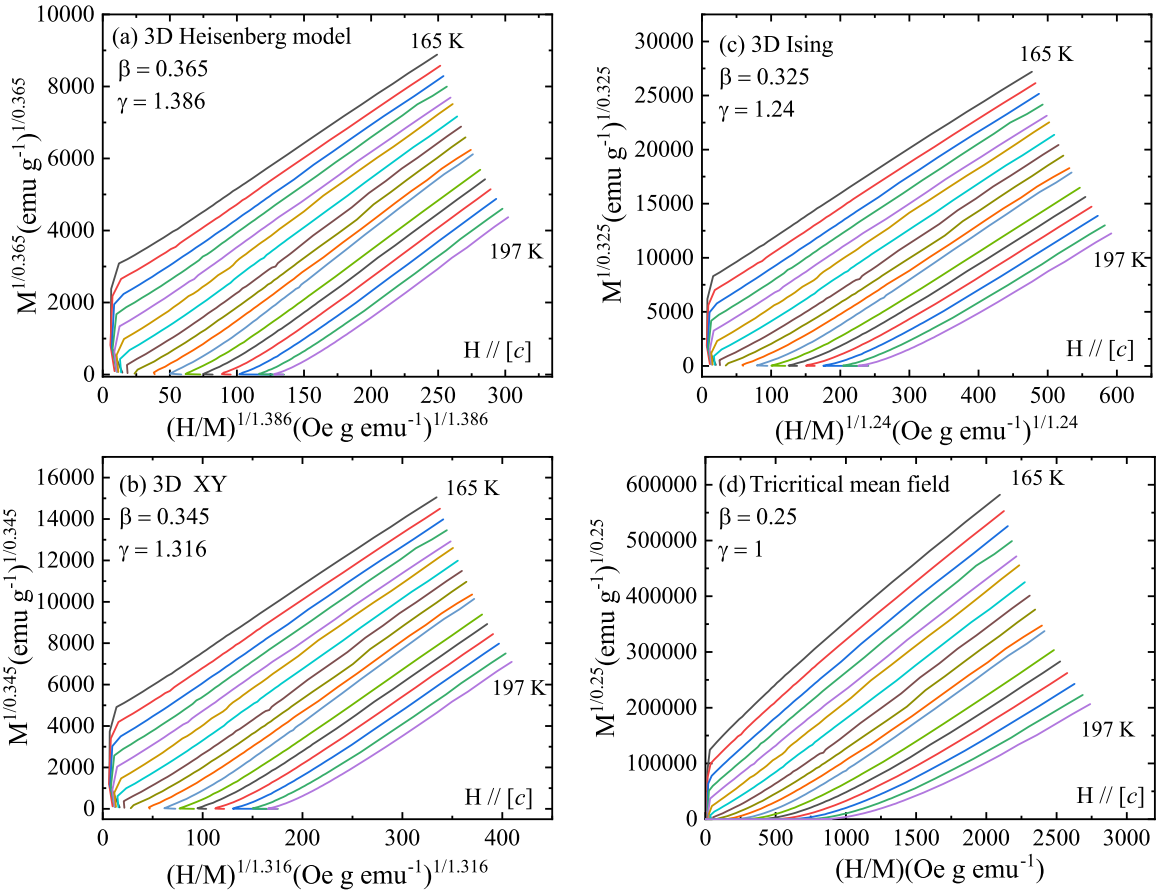

FIG. 8. Construction of the modified Arrott plots (MAP), i.e., $M^{1/\beta}$ vs $(H/M)^{1/\gamma}$ from isothermal magnetization data of F3GT crystal for different classes of theoretical models of (a) 3D Heisenberg, (b) 3D XY, (c) 3D Ising, and (d) tricritical mean field theories.

system, the modified Arrott plots (MAP) have been employed. In order to obtain an appropriate model for this system, four different sets of critical exponents corresponding to four theoretical models have been used [60,62–67]. The MAP for these four theoretical models, three-dimensional (3D) Heisenberg model with $\beta = 0.365$ and $\gamma = 1.386$, 3D Ising model with $\beta = 0.325$ and $\gamma = 1.24$, 3D XY model with $\beta = 0.345$ and $\gamma = 1.316$, and tricritical mean field model with $\beta = 0.25$ and $\gamma = 1.0$ are shown in Figs. 8(a)–8(d). As can be observed from these plots, curves are almost a straight line and somewhat parallel except for Fig. 8(d), indicating tricritical mean field model is not applicable for the present F3GT system. Among the other three models, to obtain the best and suitable model for the starting critical exponents for F3GT system, the temperature-dependent slope of the MAP has been obtained by using the formula $S(T) = dM^{1/\beta}/d(H/M)^{1/\gamma}$ [29,30]. To obtain the parallel straight line MAP, the slope at different temperatures should almost be equal. In order to identify an appropriate model for the critical behavior study, the temperature dependence of normalized slope (NS) as defined by $\mathrm{NS}(T) = S(T)/S(T_C)$ [29–31] has been calculated for the four models which are shown in Fig. 9. The curves in MAP will be a parallel straight line when NS = 1. From Fig. 9, it can be inferred that for the present F3GT system, NS is close to 1 above T_C for the 3D Heisenberg model, thereby indicating a nearly isotropic magnetic behavior above T_C which is in line with the observed magnetic susceptibility data of this system. However, NS is close to unity for temperature below T_C for the 3D Ising model and/or 3D XY model, indicating significant enhancement of the magnetic anisotropic interaction owing to the spin fluctuation upon cooling the system below the magnetic transition.

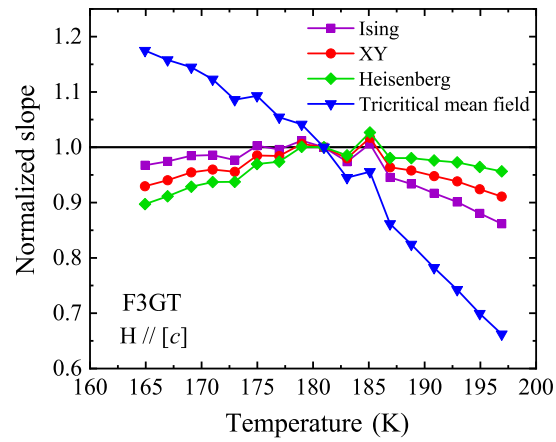

FIG. 9. Temperature-dependent normalized slope (NS) of F3GT crystal for four theoretical models as discussed in the text.

TABLE II. The comparison of the critical exponents of our CVT-grown F3GT crystal for $H \parallel [c]$ with respect to the other theoretical models and other two-dimensional van der Waals materials of interest.

Model/system	Crystal-growth method	Technique	T_C	β	γ	δ	References
Mean field		Theory		0.5	1	3	[60]
Tricritical mean field		Theory		0.25	1	5	[64]
3D Heisenberg $\{d:n\}=\{3:3\}$		Theory		0.365	1.386	4.80	[60]
3D XY $\{d:n\}=\{3:2\}$		Theory		0.345	1.316	4.81	[60]
3D Ising $\{d:n\}=\{3:1\}$		Theory		0.325	1.24	4.82	[60]
F3GT	CVT	Modified Arrott plots (MAP)	177.76 K	0.321	1.179	4.67	This work
	CVT	Kouvel-Fisher technique (KF)	177.8 K	0.325	1.183	4.64	This work
Fe_3GeTe_2	CVT	MAP	215.1 K	0.327	1.079	4.30	[29]
$Fe_{3-x}GeTe_2$	Flux	MAP	151.27 K	0.374	1.273	4.40	[30]
Fe_4GeTe_2	CVT	MAP	270.2 K	0.33	1.17	4.54	[28]
Fe_5GeTe_2	CVT	MAP	273.7 K	0.351	1.413	5.03	[31]
$CrSiTe_3$	Flux	MAP	31 K	0.170	1.532	9.92	[54]
$CrGeTe_3$	Flux	MAP	62.7 K	0.196	1.320	7.73	[55]

In order to figure out the critical exponents of the present CVT-grown F3GT more precisely, the curves of the MAP using a starting set of β and γ values are usually fitted linearly and then extrapolated to $M^{1/\beta} = 0$ and $(H/M)^{1/\gamma} = 0$ axes to obtain the temperature-dependent spontaneous magnetization $M_S(T)$ and initial magnetic susceptibility $\chi_0(T)$. Then the temperature variations of $M_S(T)$ and $\chi_0(T)$ are fitted to the power laws associated with Eqs. (3) and (4), respectively, to determine the new values of critical exponents β and γ, respectively, which are then used to reconstruct the MAP, the plot of $M^{1/\beta}$ vs $(H/M)^{1/\gamma}$. The above same exercise can be repeated to obtain new set of β and γ values and again new MAP. This rigorous iteration process needs to be performed until the obtained new values of critical exponents β and γ are stable and converge. The stable values of critical exponents β and γ are then employed to reconstruct the final MAP. From this analysis one can determine the precise value of T_C of the material [28–31,51–57]. After a rigorous iterative method of MAP of F3GT crystal for the data of $H \parallel [c]$, the finally obtained values of stable critical exponent are found to be $\beta = 0.321(8)$, $\gamma = 1.179(6)$, and $T_C = 177.76(9)$ K. The temperature variations of final spontaneous magnetization $M_S(T)$ and initial magnetic susceptibility $\chi_0(T)$ of F3GT for $H \parallel [c]$ are displayed in Fig. 10(a). The accuracy and reliability of the obtained critical exponents can be figured out by an alternate method proposed by Kouvel and Fisher [68]. According to the Kouvel-Fisher method, the temperature variation of $M_S(dM_S/dT)^{-1}$ and $\chi_0^{-1}(d\chi_0^{-1}/dT)^{-1}$ should possess straight lines with slopes equal to $(1/\beta)$ and $(1/\gamma)$, respectively, and the intercepts on the temperature axis of the lines give the transition temperature T_C. The final temperature dependence of $M_S(dM_S/dT)^{-1}$ and $\chi_0^{-1}(d\chi_0^{-1}/dT)^{-1}$ of F3GT for $H \parallel [c]$ are shown in Fig. 10(b). From the analysis using the Kouvel-Fisher technique for F3GT crystal for the data of $H \parallel [c]$, the finally obtained values of stable critical exponents are found to be $\beta = 0.325(1)$, $\gamma = 1.183(1)$, and $T_C = 177.8(2)$ K. The other critical exponent δ can be calculated using the value of critical exponents β and γ using Widom scaling relation for ferromagnetic materials as

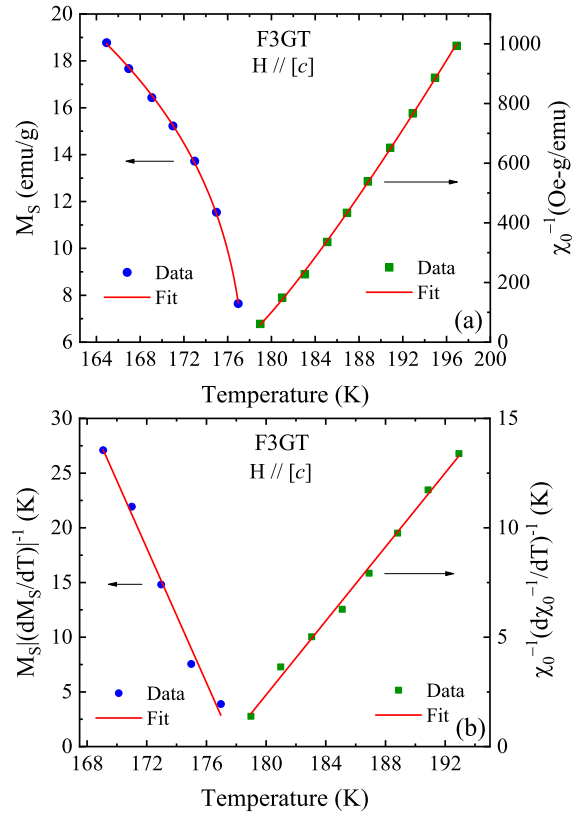

FIG. 10. (a) Temperature dependence of spontaneous magnetization and corresponding data fitting (red solid line) to the scaling Eq. (3) for $T < T_C$ to estimate critical exponent β of F3GT crystal (left scale). Temperature dependence of inverse of initial magnetic susceptibility and corresponding data fitting (red solid line) to the scaling Eq. (4) for $T > T_C$ to estimate critical exponent γ of F3GT crystal (right scale). (b) Temperature dependence of $M_S(dM_S/dT)^{-1}$ and corresponding linear data fitting (red solid line) for $T < T_C$ to estimate critical exponent β of F3GT crystal (left scale). Temperature dependence of $\chi_0^{-1}(d\chi_0^{-1}/dT)^{-1}$ and corresponding linear data fitting (red solid line) for $T > T_C$ to estimate critical exponent γ of F3GT crystal (right scale).

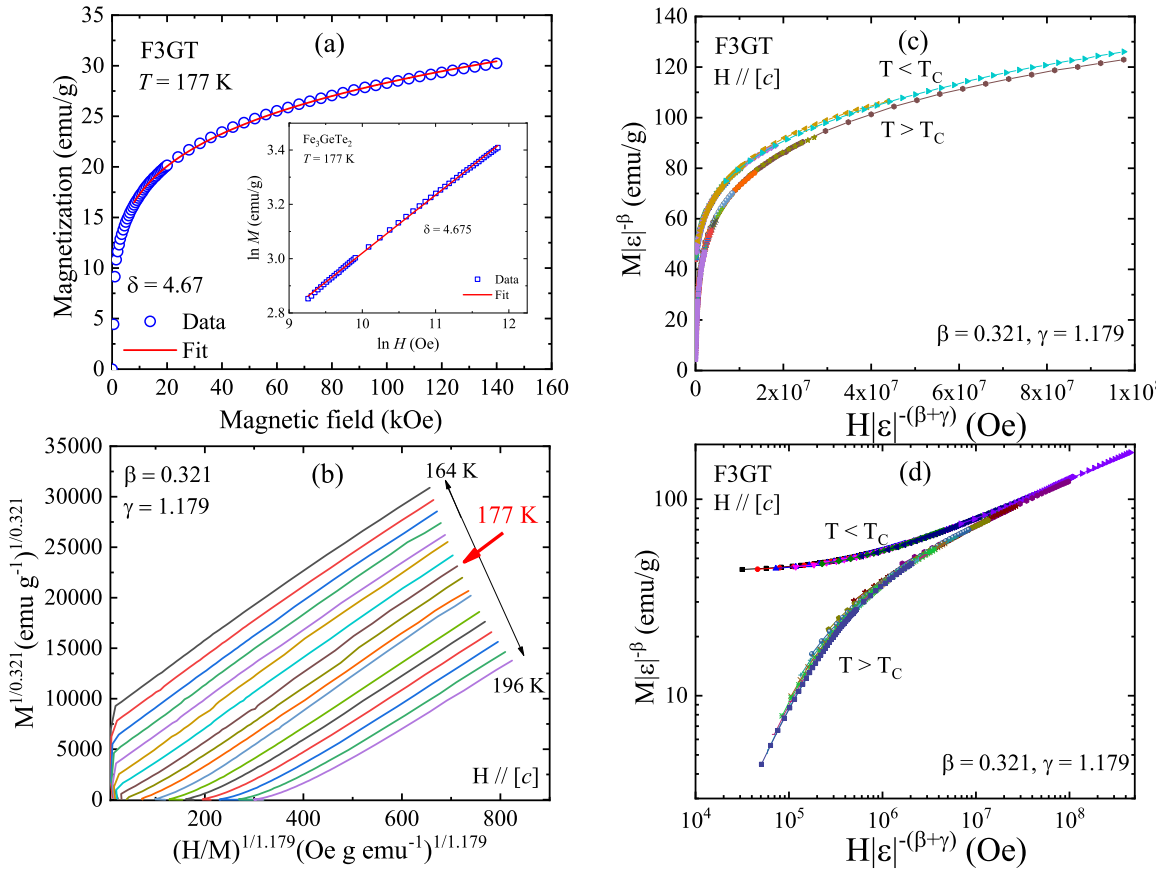

FIG. 11. (a) Magnetic field variation of isothermal magnetization at 177 K (T_C) of the F3GT crystal for $H \parallel [c]$ and data fitting to the equation of scaling hypothesis [Eq. (5)] which resulted the estimation critical exponent δ (inset of figure shows the log-log plot of M vs H at 177 K of F3GT). (b) The final MAP of F3GT crystal for $H \parallel [c]$ by using the estimated stable values of β and γ. (c) The plot of renormalized magnetization vs renormalized magnetic field of F3GT crystal for $H \parallel [c]$ by using the estimated stable values of β and γ and transition temperature by following Eq. (6) for $T < T_C$ and $T > T_C$. (d) The log-log scale plot of renormalized magnetization vs renormalized magnetic field of F3GT crystal for $H \parallel [c]$.

given by [62,69]

$$\delta = 1 + \frac{\gamma}{\beta}. \tag{9}$$

Using the values of β and γ obtained from the MAP analysis, the calculated value of $\delta = 4.67$. The value of critical exponent δ of CVT-grown F3GT crystal for $H \parallel [c]$ can be estimated from the isothermal magnetization curve at $T_C \sim 177$ K by fitting to Eq. (5) as shown in Fig. 11(a). The same can also be obtained from the the log-log scale plot of isothermal magnetization curve taken at 177 K [as shown in the inset of Fig. 11(a)]. From the fitting the obtained value of $\delta \sim 4.67(1)$ which is similar to that obtained from calculation using Widom scaling relation, indicating the reliability and accuracy of the obtained value of the critical exponents of the present F3GT crystal within the experimental precision. The obtained value of δ of present F3GT crystal is nearly equal to the theoretically calculated δ for 3D Ising, 3D XY, and 3D Heisenberg models (as can be seen in Table II) [60,63–66].

The MAP data of our CVT-grown F3GT crystal using the obtained stable values of β and γ are depicted in Fig. 11(b) which displays a set of parallel straight lines and the line corresponds to the magnetic isotherms at 177 K near T_C passes almost through the origin. The reliability and the accuracy of the obtained critical exponents and the transition temperature can further be confirmed by scaling the isothermal magnetization curves in terms of the scaling hypothesis in the asymptotic critical regime [50]. According to this scaling hypothesis, in the critical regime, the construction of the data of renormalized magnetization $m \equiv \epsilon^{-\beta} M(H, \epsilon)$ and renormalized magnetic field $h \equiv \epsilon^{-(\gamma+\beta)} H$ from isothermal magnetization data by using the obtained stable critical exponents and the critical temperature by following the magnetic equation of state as given by Eq. (6) would collapse all the data near the critical regime into two branches of universal curves wherein all the data below T_C collapse onto a curve f_- and all the data above T_C collapse onto a curve f_+ [50]. Rescaled isothermal magnetization data are displayed in Fig. 11(c) and the same in the log-log scale are shown in Fig. 11(d). As is evident from both the displayed figures that all the experimental isothermal magnetization data of CVT-grown F3GT crystal scale to the two branches of universal curves validating the scaling hypothesis. The estimated values of critical exponents and critical temperature of our CVT-grown F3GT single crystal by the MAP and Kouvel-Fisher techniques are tabulated in Table II and further compared with the theoretically predicted values for different models as well as the experimentally obtained values of other related two-dimensional van der Waals

bonded layered materials of interests as shown in Table II [28–31,54,55,60,63–66]. It can observed from Table II that the obtained critical exponents of F3GT do not belong to any particular conventional universality classes. The estimated β of F3GT is nearly equal to that of 3D Ising model which might corroborate with the large magnetocrystalline anisotropy in the F3GT crystal. The estimated γ is somewhat close to or in-between the value of γ for mean field, tricritical mean field, and 3D Ising models. This could be attributed to the extended type of exchange interaction originated from the exchange interaction of spin system beyond the nearest neighbors. Hence, it is important to understand the nature, dimensionality, and the range of exchange interaction in the F3GT system. According to the renormalization group theory, the exchange interaction between the magnetic spins for itinerant electrons decays spatially with distance r as $J(r) \approx r^{-(d+\sigma)}$, where d is spatial dimensionality and σ is a positive constant representing the range of the exchange interaction [70]. Following this model, the magnetic exchange interaction between the spins is long-range and short-range type when $\sigma < 2$ and >2, respectively. Based on this renormalization group theory, the critical exponent γ which is calculated from the initial magnetic susceptibility can be predicted by the following relationship [28–31,54–57,70]:

$$\gamma = 1 + \frac{4(n+2)}{d(n+8)}\Delta\sigma + \frac{8(n+2)(n-4)}{d^2(n+8)^2}\left[1 + \frac{2G\left(\frac{d}{2}\right)(7n+20)}{(n-4)(n+8)}\right]\Delta\sigma^2, \tag{10}$$

where $\Delta\sigma = (\sigma - d/2)$ and $G(d/2) = 3 - (1/4)(d/2)^2$, and n and d represent the spin and the lattice dimensionality of the system, respectively. The estimation of the value of σ can be obtained for a set of $\{d : n\}$ to yield the estimated stable value of γ obtained for the F3GT crystal from MAP and KF analysis. The obtained value of σ can be used to obtain the other remaining critical exponents of the system by using the following relationships: $\nu = \gamma/\sigma$, $\alpha = 2 - \nu d$, $\beta = (2 - \alpha - \gamma)/2$, and $\delta = 1 + (\gamma/\beta)$ [28–31,54–57,62–67]. The calculation of σ has been performed for a set of $\{d : n\}$ to get the experimentally obtained stable γ of the F3GT system which indicates that the best-suited value of σ is equal to 1.74 for $\{3 : 3\}$. Hence, the magnetic exchange interaction decays spatially slower than $r^{-4.74}$ which is comparable to $r^{-4.6}$ and $r^{-4.89}$ for the Fe_3GeTe_2 system with and without vacancy [29,30]. This obtained value lies between the value obtained for mean field and 3D Heisenberg models. It is a well-known fact that while the mean field theory model contributes to the long-range-type magnetic exchange interaction, the 3D Heisenberg model attributes to the short-range-type interaction. It is to be mentioned here that Taroni *et al.* carried out a comprehensive study of critical phenomena on 2D magnets and concluded that for a 2D magnetic system the value of critical exponent β should lie in the range of $0.1 \leqslant \beta \leqslant 0.25$ [71]. The studied CVT-grown F3GT being a van der Waals bonded layered material resulted a β value, indicating 3D magnetic system. This could be attributed to the small van der Waals gap and a large cleavage energy associated with the F3GT system [29]. Hence, the obtained range and dimensionality of exchange interaction in the F3GT system indicates a 3D long-range-type magnetic exchange interaction. The calculated value of β from the σ is slightly large as compared to the experimentally obtained value which could be attributed to the itinerant nature of the iron $3d$-electron magnetic spins in the system.

In order to discuss more about the nature of itinerant electron ferromagnetism in the studied CVT-grown F3GT crystal, the isothermal magnetization data taken at T_C has been analyzed based on the self-consistent renormalization (SCR) theory of spin fluctuations proposed by Takahashi [72–74]. As per this theory, magnetization M at T_C follows this relationship as given below:

$$M^4 = \frac{1}{4.671}\left(\frac{T_C^2}{T_A^3}\right)\left(\frac{H}{M}\right). \tag{11}$$

In the above relationship, M and H are in μ_B/mol Fe and Oe units, respectively. The parameter T_A in temperature unit represents the dispersion of spin fluctuation spectrum in the wave-vector space. The plot of M^4 vs H/M should possess a straight line with a slope from which one can figure out the value of the parameter T_A (as shown in Fig. 12). The linear fit of the data yield a slope value of 6.068×10^{-6} [$(\mu_B$/mol Fe$)^5$/Oe]. The calculated T_A from this slope assumes a value 1034.7 K. According to SCR theory of spin fluctuations [74], T_C of a system is related to T_A by the the following relationship:

$$T_C = (60c)^{-3/4} P_S^{3/2} T_A^{3/4} T_0^{1/4}, \tag{12}$$

where c takes a value of 0.3353, P_S is the spontaneous magnetization of the system in magnetic ground state in the unit of μ_B/mol Fe, and T_0 in temperature unit is the dispersion of spin fluctuation spectrum in the energy space. Using the values of T_C, P_S, and the estimated value of T_A, the calculated

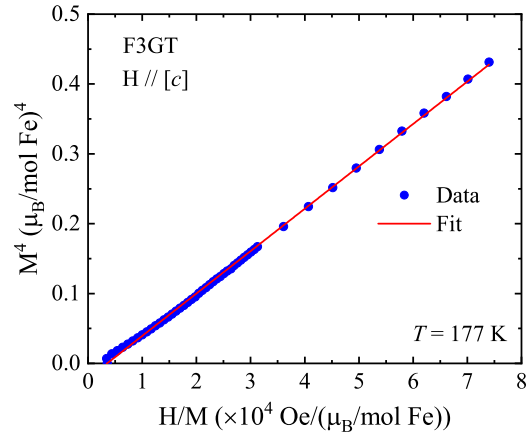

FIG. 12. The plot of M^4 vs H/M of the F3GT crystal when field applied along the crystallographic c direction.

value of T_0 of present CVT-grown F3GT is 2197.7 K. Based on the SCR theory of spin fluctuations of a magnetic system, the ratio of T_C to T_0 (T_C/T_0) governs the degree of itinerancy or localization of magnetic spins of the system. For a magnetic system having localized moments the ratio $T_C/T_0 \sim 1$ and the ratio $T_C/T_0 \ll 1$ indicates the strong itinerant character of the iron 3*d* electrons of the system. For the present F3GT system, T_C/T_0 assumes a value ~0.08 which is very much comparable to that obtained for Fe_3GeTe_2 ($T_C/T_0 = 0.096$) without iron vacancy [24], thereby indicating a weak itinerancy of the 3*d* electrons in the present F3GT system. This finding also corroborates with the Rhodes-Wohlfarth ratio (RWR) estimated for present F3GT (discussed in magnetization studies section). The ratio T_C/T_0 of the present F3GT crystal is also comparable to that of the other weak itinerant electron systems, for example, Fe_4GeTe_2 (0.16) [28], $Fe_{0.77}Co_{0.23}Si$ (0.1), and MnSi (0.13) [74]. Thus, in a nutshell, the CVT-grown F3GT single crystal exhibits 3D Heisenberg-type weak itinerant ferromagnetic long-range magnetic interaction due to itinerant electrons, wherein magnetic exchange interaction decays spatially slower than $r^{-4.74}$.

IV. SUMMARY

In summary, a comprehensive study of structural, dc, and ac magnetic susceptibility, magnetocaloric effect, room-temperature Raman spectroscopy, room-temperature Mössbauer spectroscopy, detailed critical behavior, nature of magnetic interaction of F3GT single crystal grown by chemical vapor transport (CVT) method have been investigated and reported. CVT-grown F3GT crystal crystallizes in hexagonal crystal structure with space group $P6_3/mmc$ (No. 194). Room-temperature Raman spectroscopic studies reveal phase purity and good crystalline nature of grown F3GT crystal. Room-temperature Mössbauer spectrum of present F3GT powders revealed an asymmetric doublet having broadened parts depicting paramagnetic nature and also revealed the presence of three asymmetric paramagnetic doublets in the data which corroborate the structure of F3GT. The dc magnetization and isothermal magnetization studies on the CVT-grown F3GT crystal reveal the occurrence of a ferromagnetic to paramagnetic transition at 178.4 K (T_C), the crystallographic *c* axis being the easy magnetization direction. The magnetocaloric effect of the F3GT single crystal estimated in terms of isothermal magnetic entropy change (ΔS_m) exhibits anisotropic behavior and resulted ΔS_m^{max} of the F3GT crystal are ≈ -2.4 J/kg K and ≈ -2.6 J/kg K for $\Delta H = 100$ kOe for $H \parallel [ab]$ and $H \parallel [c]$, respectively. The nature of magnetocaloric curves and the Arrott plots of the F3GT crystal depict the occurrence of a second-order ferromagnetic to paramagnetic transition at T_C. Critical behavior analyses of the F3GT crystal in the close vicinity of T_C by modified Arrott plots (MAP) yield the critical exponents $\beta = 0.321$, $\gamma = 1.179$, and $\delta = 4.67$ and by using the Kouvel-Fisher (KF) technique, the critical exponents are found to be $\beta = 0.325$, $\gamma = 1.183$, and $\delta = 4.64$. The critical magnetization isotherm at T_C reveals the critical exponent δ to be 4.67. The estimated critical exponents of the F3GT crystal obey the scaling hypothesis and the isothermal magnetization curves at different temperatures scale onto the two branches of the universal curve. Overall analyses of the critical behavior study suggest a 3D Heisenberg-type weak itinerant ferromagnetic long-range magnetic interaction due to itinerant electrons wherein magnetic exchange interaction decays spatially slower than $r^{-4.74}$ in the van der Waals bonded layered F3GT single crystal. This work is expected to stimulate the investigation of the nature of magnetic exchange interaction in materials with different iron concentrations and materials with even lower dimensions for futuristic spintronics applications in the era of rapid development of two-dimensional van der Waals materials.

ACKNOWLEDGMENT

The authors thank Dr. P. V. Rajesh, B. K. Behera, and Mukesh Kumar, UGC-DAE Consortium for Scientific Research, Kolkata Centre, for the help during the experiments.

[1] A. K. Geim and I. V. Grigorieva, Nature (London) **499**, 419 (2013).
[2] N. Sivadas, M. W. Daniels, R. H. Swendsen, S. Okamoto, and D. Xiao, Phys. Rev. B **91**, 235425 (2015).
[3] X. Li and J. Yang, J. Mater. Chem. C **2**, 7071 (2014).
[4] M. W. Lin, H. L. Zhuang, J. Q. Yan, T. Z. Ward, A. A. Puretzky, C. M. Rouleau, Z. Gai, L. B. Liang, V. Meunier, B. G. Sumpter, P. Ganesh, P. R. C. Kent, D. B. Geohegan, D. G. Mandrus, and K. Xiao, J. Mater. Chem. C **4**, 315 (2016).
[5] X. Zhang, Y. L. Zhao, Q. Song, S. Jia, J. Shi, and W. Han, Jpn. J. Appl. Phys. **55**, 033001 (2016).
[6] L. D. Casto, A. J. Clune, M. O. Yokosuk, J. L. Musfeldt, T. J. Williams, H. L. Zhuang, M.-W. Lin, K. Xiao, R. G. Hennig, B. C. Sales, J.-Q. Yan, and D. Mandrus, APL Mater. **3**, 041515 (2015).
[7] M. Chhowalla, H. S. Shin, G. Eda, L.-J. Li, K. P. Loh, and H. Zhang, Nat. Chem. **5**, 263 (2013).
[8] S. Z. Butler, S. M. Hollen, L. Cao, Y. Cui, J. A. Gupta, H. R. Gutiérrez, T. F. Heinz, S. S. Hong, J. Huang, and A. F. Ismach, ACS Nano **7**, 2898 (2013).
[9] G. R. Bhimanapati, Z. Lin, V. Meunier, Y. Jung, J. Cha, S. Das, D. Xiao, Y. Son, M. S. Strano, V. R. Cooper, L. Liang, S. G. Louie, E. Ringe, W. Zhou, S. S. Kim, R. R. Naik, B. G. Sumpter, H. Terrones, F. Xia, Y. Wang *et al.*, ACS Nano **9**, 11509 (2015).
[10] J.-X. Zhu, M. Janoschek, D. S. Chaves, J. C. Cezar, T. Durakiewicz, F. Ronning, Y. Sassa, M. Mansson, B. L. Scott, N. Wakeham, E. D. Bauer, and J. D. Thompson, Phys. Rev. B **93**, 144404 (2016).
[11] Y. Wang, C. Xian, J. Wang, B. Liu, L. Ling, L. Zhang, L. Cao, Z. Qu, and Y. Xiong, Phys. Rev. B **96**, 134428 (2017).
[12] Y. Zhang, H. Lu, X. Zhu, S. Tan, W. Feng, Q. Liu, W. Zhang, Q. Chen, Y. Liu, X. Luo, D. Xie, L. Luo, Z. Zhang, X. Lai, Sci. Adv. **4**, eaao6791 (2018).
[13] G. D. Nguyen, J. Lee, T. Berlijn, Q. Zou, S. M. Hus, J. Park, Z. Gai, C. Lee, and A.-P. Li, Phys. Rev. B **97**, 014425 (2018).
[14] J.-G. Park, J. Phys.: Condens. Matter **28**, 301001 (2016).
[15] D. L. Duong, S. J. Yun, and Y. H. Lee, ACS Nano **11**, 11803 (2017).

[16] K. S. Burch, D. Mandrus, and J.-G. Park, Nature (London) **563**, 47 (2018).
[17] C. Gong, L. Li, Z. Li, H. Ji, A. Stern, Y. Xia, T. Cao, W. Bao, C. Wang, Y. Wang, Z. Q. Qiu, R. J. Cava, S. G. Louie, J. Xia, and X. Zhang, Nature (London) **546**, 265 (2017).
[18] N. D. Mermin and H. Wagner, Phys. Rev. Lett. **17**, 1133 (1966).
[19] F. Xue, Y. Hou, Z. W., and R. Wu, Phys. Rev. B **100**, 224429 (2019).
[20] Zhe Wang, M. Gibertini, D. Dumcenco, T. Taniguchi, K. Watanabe, E. Giannini, and A. F. Morpurgo, Nat. Nanotechnol. **14**, 1116 (2019).
[21] L. Webster, and J.-A. Yan, Phys. Rev. B **98**, 144411 (2018).
[22] T. Li, S. Jiang, N. Sivadas, Z. Wang, Y. Xu, D. Weber, J. E. Goldberger, K. Watanabe, T. Taniguchi, C. J. Fennie, K. F. Mak, and J. Shan, Nat. Mater. **18**, 1303 (2019).
[23] C. Zhang, L. Wang, Y. Gu, X. Zhang, X. Xia, S. Jiang, Liang-Long Huang, Y. Fu, C. Liu, J. Lin, X. Zou, H. Su, J.-W. Mei, and J.-F. Dai, Nanoscale **14**, 5851 (2022).
[24] B. Chen, J. Yang, H. Wang, M. Imai, H. Ohta, C. Michioka, K. Yoshimura, and M. Fang, J. Phys. Soc. Jpn. **82**, 124711 (2013).
[25] A. F. May, S. Calder, C. Cantoni, H. Cao, and M. A. McGuire, Phys. Rev. B **93**, 014411 (2016).
[26] A. F. May, D. Ovchinnikov, Q. Zheng, R. Hermann, S. Calder, B. Huang, Z. Fei, Y. Liu, X. Xu, and M. A McGuire, ACS Nano **13**, 4436 (2019).
[27] A. F. May, M.-H. Du, V. R. Cooper, and M. A. McGuire, Phys. Rev. Mater. **4**, 074008 (2020).
[28] S. Mondal, N. Khan, S. M. Mishra, B. Satpati, and P. Mandal, Phys. Rev. B **104**, 094405 (2021).
[29] B. Liu, Y. Zou, S. Zhou, L. Zhang, Z. Wang, H. Li, Z. Qu, and Y. Zhang, Sci. Rep. **7**, 6184 (2016).
[30] Y. Liu, V. N. Ivanovski, and C. Petrovic, Phys. Rev. B **96**, 144429 (2017).
[31] Z. Li, W. Xia, H. Su, Z. Yu, Y. Fu, L. Chen, X. Wang, N. Yu, Z. Zou, and Y. Guo, Sci. Rep. **10**, 15345 (2020).
[32] H.-J. Deiseroth, K. Aleksandrov, C. Reiner, L. Kienle, and R. K. Kremer, Eur. J. Inorg. Chem. **2006**, 1561 (2006).
[33] L. Du, J. Tang, Y. Zhao, X. Li, R. Yang, X. Hu, X. Y. Bai, X. Wang, K. Watanabe, T. Taniguchi, D. Shi, G. Yu, X. Bai, T. Hasan, G. Zhang, and Z. Sun, Adv. Funct. Mater. **29**, 1904734 (2019).
[34] A. Milosavljević, A. Šolajić, S. Djurdjić-Mijin, J. Pešić, B. Višić, Y. Liu, C. Petrovic, N. Lazarević, and Z. V. Popović, Phys. Rev. B **99**, 214304 (2019).
[35] V. Y. Verchenko, A. A. Tsirlin, A. V. Sobolev, I. A. Presniakov, and A. V. Shevelkov, Inorg. Chem. **54**, 8598 (2015).
[36] J. Yi, H. Zhuang, Q. Zou, Z. Wu, G. Cao, S. Tang, S. A. Calder, P. R. C. Kent, D. Mandrus, and Z. Gai, 2D Mater. **4**, 011005 (2017).
[37] S. Bao, W. Wang, Y. Shangguan, Z. Cai, Zhao-Yang Dong, Z. Huang, W. Si, Z. Ma, R. Kajimoto, K. Ikeuchi, S.-I. Yano, S.-L. Yu, X. Wan, J.-X. Li, and J. Wen, Phys. Rev. X **12**, 011022 (2022).
[38] X. Bai, F. Lechermann, Y. Liu, Y. Cheng, A. I. Kolesnikov, F. Ye, T. J. Williams, S. Chi, T. Hong, G. E. Granroth, A. F. May, and S. Calder, Phys. Rev. B **106**, L180409 (2022).
[39] E. P. Wohlfarth, J. Magn. Magn. Mater. **7**, 113 (1978).
[40] T. Moriya, J. Magn. Magn. Mater. **14**, 1 (1979).
[41] V. K. Pecharsky, and K. A. Gschneidner Jr., Int. J. Refrig. **29**, 1239 (2006).
[42] R. Mondal, R. Nirmala, J. Arout Chelvane, and S. K. Malik, J. Magn. Magn. Mater. **393**, 376 (2015).
[43] R. Mondal, R. Kulkarni, and A. Thamizhavel, J. Magn. Magn. Mater. **483**, 27 (2019).
[44] Y. Liu, J. Li, J. Tao, Y. Zhu, and C. Petrovic, Sci. Rep. **9**, 13233 (2019).
[45] Y. Liu and C. Petrovic, Phys. Rev. Mater. **3**, 014001 (2019).
[46] Y. Liu and C. Petrovic, Phys. Rev. B **97**, 174418 (2018).
[47] X. Yu, X. Zhang, Q. Shi, S. Tian, H. Lei, K. Xu, and H. Hosono, Front. Phys. **14**, 43501 (2019).
[48] L.-Z. Zhang, A.-L. Zhang, X.-D. He, X.-W. Ben, Q.-L. Xiao, W.-L. Lu, F. Chen, Z. Feng, S. Cao, J. Zhang, and J.-Y. Ge, Phys. Rev. B **101**, 214413 (2020).
[49] H. E. Stanley, *Introduction to Phase Transition and Critical Phenomena* (Oxford University Press, New York, 1971).
[50] M. E. Fisher, Rep. Prog. Phys. **30**, 615 (1967).
[51] Y. Su, Y. Sui, J.-G. Cheng, J.-S. Zhou, X. Wang, Y. Wang, and J. B. Goodenough, Phys. Rev. B **87**, 195102 (2013).
[52] M. Halder, S. M. Yusuf, M. D. Mukadam, and K. Shashikala, Phys. Rev. B **81**, 174402 (2010).
[53] A. K. Pramanik and A. Banerjee, Phys. Rev. B **79**, 214426 (2009).
[54] B. Liu, Y. Zou, L. Zhang, S. Zhou, Z. Wang, W. Wang, Z. Qu, and Y. Zhang, Sci. Rep. **6**, 33873 (2016).
[55] Y. Liu, and C. Petrovic, Phys. Rev. B **96**, 054406 (2017).
[56] G. T. Lin, H. L. Zhuang, X. Luo, B. J. Liu, F. C. Chen, J. Yan, Y. Sun, J. Zhou, W. J. Lu, P. Tong, Z. G. Sheng, Z. Qu, W. H. Song, X. B. Zhu, and Y. P. Sun, Phys. Rev. B **95**, 245212 (2017).
[57] Y. Liu, and C. Petrovic, Phys. Rev. B **96**, 134410 (2017).
[58] D. Kim, B. L. Zink, F. Hellman, and J. M. D. Coey, Phys. Rev. B **65**, 214424 (2002).
[59] A. Arrott, Phys. Rev. **108**, 1394 (1957).
[60] B. K. Banerjee, Phys. Lett. **12**, 16 (1964).
[61] A. Arrott and J. E. Noakes, Phys. Rev. Lett. **19**, 786 (1967).
[62] L. P. Kadanoff, Phys. Phys. Fiz. **2**, 263 (1966).
[63] M. E. Fisher, S.-K. Ma, and B. G. Nickel, Phys. Rev. Lett. **29**, 917 (1972).
[64] J. C. LeGuillou and J. Zinn-Justin, Phys. Rev. B **21**, 3976 (1980).
[65] S. N. Kaul, J. Magn. Magn. Mater. **53**, 5 (1985).
[66] K. Huang, *Statistical Mechanics*, 2nd ed. (Wiley, New York, 1987).
[67] S. F. Fischer, S. N. Kaul, and H. Kronmüller, Phys. Rev. B **65**, 064443 (2002).
[68] J. S. Kouvel and M. E. Fisher, Phys. Rev. **136**, A1626 (1964).
[69] B. Widom, J. Chem. Phys. **43**, 3898 (1965).
[70] A. Pelissetto and E. Vicari, Phys. Rep. **368**, 549 (2002).
[71] A. Taroni, S. T. Bramwell, and P. C. W. Holdsworth, J. Phys.: Condens. Matter **20**, 275233 (2008).
[72] T. Moriya and Y. Takahashi, J. Phys. Soc. Jpn. **45**, 397 (1978).
[73] Y. Takahashi, J. Phys. Soc. Jpn. **55**, 3553 (1986).
[74] Y. Takahashi, *Spin Fluctuation Theory of Itinerant Electron Magnetism* (Springer, Berlin, 2013).